CHEMSUSCHEM

ChemPubSoc Europe

DOI: 10.1002/cssc.201200587

Mesoporous Siliconiobium Phosphate as a Pure Brønsted Acid Catalyst with Excellent Performance for the Dehydration of Glycerol to Acrolein

Youngbo Choi, Dae Sung Park, Hyeong Jin Yun, Jayeon Baek, Danim Yun, and Jongheop Yi*[a]

The development of solid acid catalysts that contain a high density of Brønsted acid sites with suitable acidity, as well as a long lifetime, is one of great challenges for the efficient dehydration of glycerol to acrolein. Herein, we report on a mesoporous siliconiobium phosphate (NbPSi-0.5) composite, which is a promising solid Brønsted acid that is a potential candidate for such a high-performance catalyst. A variety of characterization results confirm that NbPSi-0.5 contains nearly pure Brønsted acid sites and has well-defined large mesopores. In addition, NbPSi-0.5 contains a similar amount of acid sites and exhibits weaker acidity than that of the highly acidic niobium phosphate and HZSM-5 zeolite. NbPSi-0.5 is quite stable and has a high activity for the dehydration of glycerol. The stability of NbPSi-0.5 is about three times higher than that of the reported catalyst. The significantly enhanced catalytic performance of NbPSi-0.5 can be attributed to 1) nearly pure Brønsted acidity, which suppresses side reactions that lead to coke formation; 2) a significant reduction of pore blocking due to the mesopores; and 3) a decrease in the amount and oxidation temperature of coke.

Introduction

Solid acids play key roles in the petrochemical industry by catalyzing important conversion reactions of hydrocarbons. The recent increase in efforts to utilize biomass as a renewable resource are expanding the importance and utility of solid acid catalysts, since acid-catalyzed reactions, such as dehydration and hydrogenolysis, can provide efficient pathways for the conversion of biomass into valuable products.[1,2] However, the oxygen content of biobased chemicals is typically higher than that of the corresponding hydrocarbons.[3] This places new requirements on the use of solid acid catalysts for biomass conversion.[4,5]

The dehydration of glycerol, which is a major byproduct in the manufacture of biodiesel, is one of the intensively studied examples in which solid acid catalysts can be utilized for the transformation of biobased feedstock. The acid-catalyzed dehydration of glycerol leads to the production of acrolein, which is a versatile chemical in the production of acrylic acid and polyesters as well as in the agrochemical industry.[6–8]

For this reaction, numerous heterogeneous acid catalysts, including zeolites,[9–13] heteropolyacids,[14–18] and metal oxides,[19–21] have been investigated. Previous studies reported important implications of this, including 1) the types of acid sites, 2) the acid strength, and 3) the stability of catalysts, which are important issues in the preparation of efficient acid catalysts.

It is generally accepted that Brønsted acid sites are superior to Lewis acid sites for the selective conversion of glycerol into acrolein.[8,10,14] Furthermore, it has been reported that a decrease in the number of Lewis acid sites has a significant effect on the stability of catalysts.[19] The beneficial effect of Brønsted acidity on catalytic efficiency has been also reported in dehydration reactions of other carbohydrates that are similar in structure to glycerol. Recently, Weingarten et al. reported that acid catalysts with a high ratio of Brønsted to Lewis acid sites were much more selective for the preparation of furfural by the dehydration of xylose.[5]

Second, catalysts with medium acidity ($-8.0 < H_0 < 3.0$) perform well in the selective conversion of glycerol into acrolein.[8] However, some contradictory results have appeared, reporting that strong[14] or weak[22] acid catalysts show the best selectivity for acrolein, thus making the selection of catalysts with the appropriate acidity somewhat controversial.

Third, overcoming the low stability of catalysts would be a significant breakthrough for practical applications. Although many of the existing acid catalysts show high catalytic activities in the early stages of reactions, they frequently become deactivated due to the deposition of coke.[6] Various approaches have been proposed to increase the stability of such catalysts. These include suppressing the rate of coking by adding O_2 or H_2 to the feed flow[14,21,23,24] and modifying the catalysts with promoters to change the acid properties of the catalysts.[16] However, these methods have not been altogether successful and clearly additional improvements are needed.

[a] Y. Choi, D. S. Park, Dr. H. J. Yun, J. Baek, D. Yun, Prof. J. Yi
World Class University Program of Chemical Convergence
for Energy & Environment, Institute of Chemical Processes
School of Chemical and Biological Engineering
Seoul National University, Seoul 151-742 (Republic of Korea)
Fax: (+82) 2-885-6670
E-mail: jyi@snu.ac.kr

Supporting Information for this article is available on the WWW under http://dx.doi.org/10.1002/cssc.201200587.

Considering these issues, therefore, the design of acid catalysts with a higher density of Brønsted acid sites with suitable acidity, as well as high resistance to deactivation, would be highly desirable.

Herein, we report on the synthesis and characterization of a mesoporous siliconiobium phosphate (NbPSi-0.5) composite, and applications as a promising solid Brønsted acid catalyst for the efficient and stable dehydration of glycerol into acrolein. Niobium phosphate (NbP) can be a good candidate as a base material for the catalyst, as it has advantages of high acidity and good water tolerance.[25,26] These properties can be beneficial to the dehydration of glycerol, which generally involves a high concentration of water. However, NbP, as is the case for most solid acids, retains both Lewis and Brønsted acidity.[27,28] This problem was approached by combining NbP with silicate to form a homogeneous composite. Generally, Lewis acid sites of NbP originate from coordinatively unsaturated Nb^{5+} ions, and these are probably related to the NbO_4 tetrahedral structure.[29,30] It is assumed that the added Si atoms, which form tetra-coordinate bonds, replace Nb atoms in lower coordination environments, leading to a decrease in the density of Lewis acid sites.

Importantly, the synthesis of NbP-based materials with mesostructures is highly challenging because the mesostructures have beneficial effects on catalytic performance.[31,32] In this study, mesoporous NbPSi-0.5 with large pores was successfully prepared by means of a solvothermal method combined with solvent evaporation. In catalytic tests for the dehydration of glycerol to acrolein, NbPSi-0.5 showed excellent activity and substantially enhanced stability in comparison with NbP, commercial zeolite (HZSM-5), and the reported long-life catalyst. Rationales for the high catalytic performance of NbPSi-0.5 are also discussed.

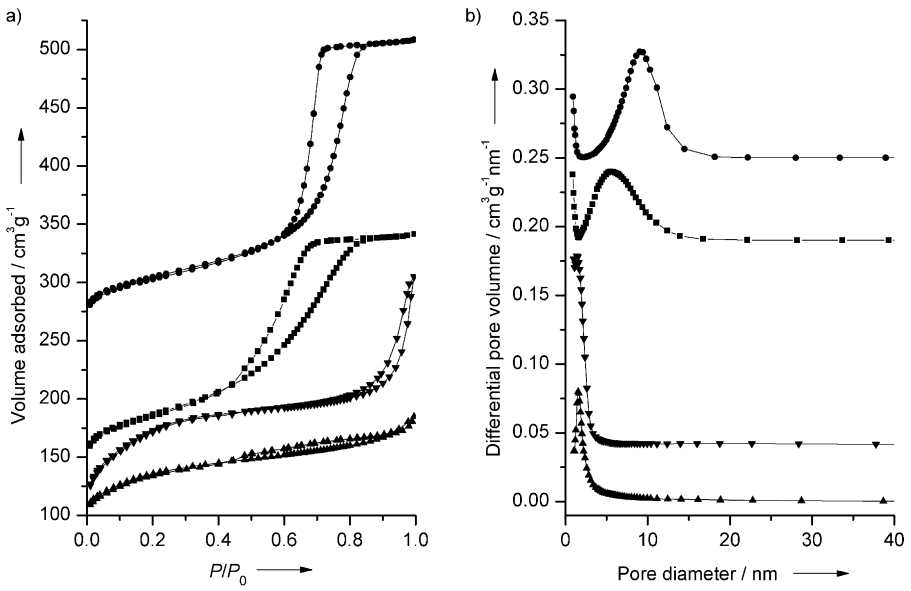

Figure 1. a) N_2 adsorption–desorption isotherms and b) Barrett–Joyner–Halenda (BJH) pore size distribution curves for NbPSi-0.5 (●), NbPSi-1 (■), NbP (▼), and HZSM-5 (▲). The isotherms for NbPSi-0.5, NbPSi-1, and NbP have been offset by 240, 130, and 70 $cm^3 g^{-1}$, respectively, and the pore size distribution curves for NbPSi-0.5, NbPSi-1, and NbP have been offset by 0.25, 0.19, and 0.04 $cm^3 g^{-1} nm^{-1}$ along the vertical axis, respectively.

Results and Discussion

Structural characterization

The N_2 adsorption–desorption isotherms and pore size distribution of NbPSi-0.5 (atomic ratio of Nb/P = 0.5; atomic ratio of Si/P = 0.5), NbP (atomic ratio of Nb/P = 1), and HZSM-5 are shown in Figure 1. For comparison, the isotherm and pore size distribution of NbPSi-1 (atomic ratio of Nb/P = 1; atomic ratio of Si/P = 0.5) are also included. NbPSi-1 was prepared by procedures identical to those of NbPSi-0.5 except for the Nb/P ratio.

The isotherm of NbPSi-0.5 was similar to a type IV isotherm and exhibited an H1-type hysteresis loop at relative pressures (P/P_0) ranging from 0.6–0.8. This indicates that NbPSi-0.5 has a well-developed mesoporous structure with large pores. The average pore size of NbPSi-0.5, calculated from the BJH adsorption branch, was about 7.2 nm and its surface area was about 238 $m^2 g^{-1}$ (Table 1). On the other hand, NbP and HZSM-5 displayed isotherms similar to type II with no significant hysteresis loops, consistent with the microporous structure of the reference catalysts.[33] The average pore sizes of NbP and

Table 1. Textural properties, atomic concentration of elements, and uptake of NH_3 for NbPSi-0.5, NbPSi-1, NbP, and HZSM-5.

Solid acid	S_{BET}[a] [$m^2 g^{-1}$]	D_{av}[b] [nm]	S_{micro}[c] [$m^2 g^{-1}$]	V_{micro}[c] [$cm^3 g^{-1}$]	V_{total}[d] [$cm^3 g^{-1}$]	Bulk atomic ratios[e] Nb/P	Bulk atomic ratios[e] Si/P	Surface atomic ratios[f] Nb/P	Surface atomic ratios[f] Si/P	NH_3 uptake[g] [$\mu mol g^{-1}$]
NbPSi-0.5	238 (56)[h]	7.2 (12.3)[h]	– (–)[h]	– (0.001)[h]	0.545 (0.172)[h]	0.53	0.51	0.48	0.54	41.5
NbPSi-1	205 (36)[h]	4.1 (14.2)[h]	– (–)[h]	– (0.002)[h]	0.329 (0.079)[h]	0.98	0.47	1.04	0.45	43.7
NbP	370 (29)[h]	< 1.5 (19)[h]	246 (10)[h]	0.092 (0.004)[h]	0.301 (0.054)[h]	1.05	–	0.97	–	46.2
HZSM-5	441 (20)[h]	< 1.5 (6.4)[h]	350 (6)[h]	0.164 (0.003)[h]	0.273 (0.038)[h]	–	–	–	–	45.6

[a] The Brunauer–Emmett–Teller (BET) surface area (S_{BET}) was calculated from the N_2 adsorption branch in the relative pressure range from 0.05 to 0.25. [b] The average pore size (D_{av}) was determined by the BJH method. [c] The micropore area (S_{micro}) and volume (V_{micro}) were obtained by the *t*-plot method. [d] Total pore volume (V_{total}) was evaluated at a relative pressure of 0.99. [e] Determined by inductively coupled plasma atomic emission spectroscopy (ICP-AES). [f] Determined by X-ray photoelectron spectroscopy (XPS). [g] Estimated from NH_3 pulse chemisorption. [h] Values in parentheses were measured after reaction for 8 h at a gas hourly space velocity (GHSV) of 14940 mL $g_{catalyst}^{-1} h^{-1}$.

HZSM-5 were less than 1.5 nm. In the case of NbPSi-1, the hysteresis loop was similar to that of NbPSi-0.5. However, the hysteresis loop of NbPSi-1 was broader and its lower end occurred at a P/P_0 value of about 0.4, indicating that NbPSi-1 has smaller pore sizes with less uniform distribution.

The pore structures were further investigated by TEM observations (Figure 2). The images clearly show that large mesopores were formed in NbPSi-0.5, and NbPSi-1 contained medium-sized mesopores. The TEM images also confirmed the microporous nature of NbP and HZSM-5. The average pore sizes, as determined from the TEM images, were in good agreement with BET results.

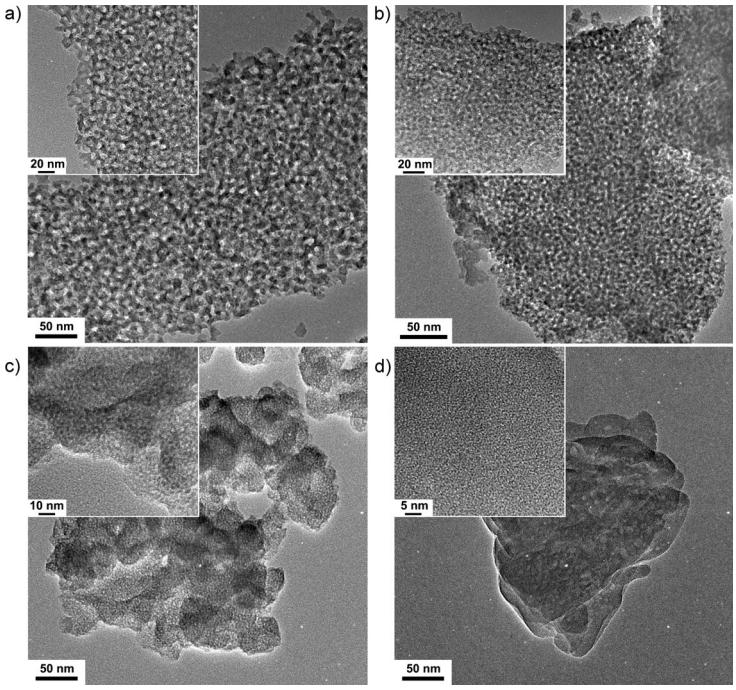

Figure 2. TEM images of a) NbPSi-0.5, b) NbPSi-1, c) NbP, and d) HZSM-5.

The concentration of elements in the bulk and surface phase of NbPSi-0.5, NbPSi-1, and NbP were measured by ICP-AES and XPS, respectively. The results of elemental analyses are shown in Table 1. The atomic ratio of Nb/P in NbPSi-0.5 was about half that for NbP. In addition, the content of Nb and Si atoms in NbPSi-0.5 was nearly the same. This indicates that approximately half of the Nb ions in NbPSi-0.5 are successfully substituted by Si ions, as expected. The atomic ratios of the bulk phase were very similar to those of the surface phase, suggesting the homogeneous distribution of elements in NbPSi-0.5. In the case of NbPSi-1, the atomic ratio of Nb/P was close to that for NbP. This implies that added Si atoms have a preference for forming separate bonds rather than substituting Nb atoms in NbPSi-1, and that NbPSi-1 has a much lower degree of substitution of Nb atoms than NbPSi-0.5.

The structure of NbP is similar to that of Nb_2O_5.[25] It is mainly composed of distorted NbO_6 octahedra and PO_4 tetrahedra,[26] and NbO_4 tetrahedra are also found in NbP-based materials.[34,35] In NbP, the terminal P–OH and Nb–OH groups function as Brønsted acids and the P–OH group is a stronger Brønsted acid than the Nb–OH group.[26] On the other hand, Lewis acidity is attributed to coordinatively unsaturated Nb^{5+} sites.[29] These coordinatively unsaturated Nb^{5+} sites are related to NbO_4 units in view of the fact that in Nb_2O_5, NbO_4 tetrahedra with Nb=O groups are Lewis acid sites.[30,36]

Based on the above, we hypothesize that the partial substitution of Nb atoms with Si atoms in NbP would lead to an increase in the ratio of Brønsted to Lewis acid sites. This is because Si occupies a tetrahedral environment and the added Si atoms would be expected to preferentially replace Nb atoms in tetrahedral environments, leading to suppression in the formation of Lewis acid sites. In addition, the properties of silica, which generates Brønsted acidity by the reaction with phosphate,[37] would also be useful in terms of increasing the number of Brønsted acid sites.

NbPSi-0.5 and NbPSi-1 have an amorphous structure similar to NbP, as shown by X-ray diffraction patterns (see Figure S1 in the Supporting Information), so structural FTIR analyses were used to further investigate the structure of NbPSi-0.5 and NbPSi-1. The results shown in Figure 3 provide some clues in support of our speculations on modifying the Lewis acid sites. The FTIR spectra for NbPSi-0.5, NbPSi-1, and NbP revealed vibrational bands at around 1220, 1020, and 510 cm^{-1} that are attributable to asymmetric and symmetric stretching of P=O, and the harmonic vibration of O–P–O, respectively.[38,39] The spectra of NbPSi-0.5 and NbPSi-1 also provided information regarding the bonding environments of Si atoms. Modes related to vibrations of asymmetric Si–O, symmetric Si–O, and O–Si–O appeared at around 1101, 800, and 468 cm^{-1}, respectively.[40] With regard to the bonding structure of Nb atoms, NbP showed two bands at around 650 and 926 cm^{-1}, which could be assigned to the stretching of Nb–O and Nb=O groups, respectively.[29,38] However, for NbPSi-0.5, a significant peak corresponding to

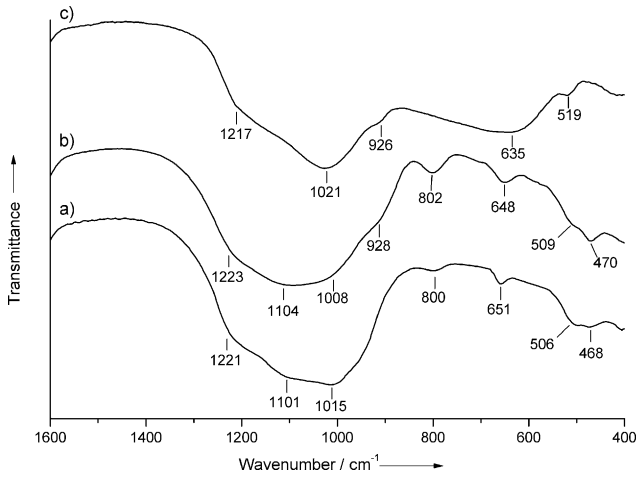

Figure 3. Structural FTIR spectra for a) NbPSi-0.5, b) NbPSi-1, and c) NbP.

Nb=O groups was not observed at a similar position. This result suggests that NbPSi-0.5 contains very small amount of Nb=O groups, which are related to Lewis acid sites. In the case of NbPSi-1, a small shoulder band corresponding to Nb=O groups appeared at around 928 cm^{-1}, similar to NbP. This suggests that Nb atoms in NbPSi-1 are not sufficiently substituted by Si atoms, and is in good agreement with the elemental analysis results.

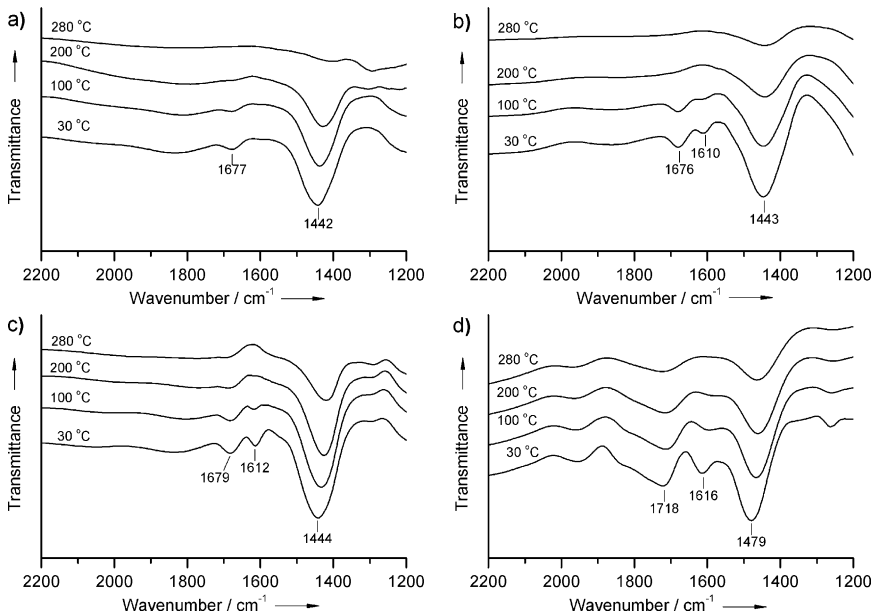

Figure 4. In situ FTIR spectra of a) NbPSi-0.5, b) NbPSi-1, c) NbP, and d) HZSM-5 for NH_3 adsorption at room temperature and desorption at different temperatures.

Characterization of acid properties

In situ FTIR measurements with ammonia were performed to distinguish between the Brønsted and Lewis acid sites in the samples. Ammonia was used as a probe molecule instead of pyridine as the small kinetic diameter of ammonia allows easy access inside the small pores of the reference samples.[41] Figure 4 shows the FTIR spectra of ammonia adsorbed on catalysts at room temperature and subsequently desorbed at increasing temperatures.

In the spectra, the peaks in the regions of 1440–1480 and 1670–1720 cm^{-1} are assigned to the symmetric and asymmetric N–H deformation of NH_4^+, which are formed by the interaction of NH_3 with the Brønsted acid sites. In addition, the peak between 1600 and 1630 cm^{-1} originates from the asymmetric N–H deformation of NH_3 coordinatively bonded to Lewis acid sites.[42] The spectra of NbP and HZSM-5 clearly demonstrated that these reference catalysts contained both Brønsted and Lewis acid sites. This is in good agreement with previous results reported in the literature.[43,44] For NbPSi-1, a peak corresponding to a Lewis acid site clearly appeared at 1610 cm^{-1}, although the size of the Lewis acid peak for NbPSi-1 was smaller than those for NbP and HZSM-5. However, in the case of NbPSi-0.5, no distinguishable peak for ammonia interacting with Lewis acid sites was observed. Thus, it can be concluded that most of the acid sites in NbPSi-0.5 are Brønsted acid sites, and these findings are entirely consistent with the structural FTIR results.

It should be noted that the IR peaks for HZSM-5 appeared at a higher frequency than those for NbPSi-0.5, NbPSi-1, and NbP. As the strength of acid sites increase, the peaks move toward higher frequencies. Therefore, these results suggest that HZSM-5 contains the strongest acid sites. Furthermore, on evacuation at 280 °C, the IR peaks for adsorbed ammonia were substantially decreased for NbPSi-0.5, whereas they still remained for NbP, NbPSi-1, and HZSM-5, indicating that ammonia was less strongly adsorbed to NbPSi-0.5 than to other catalysts.

The amount of acid sites present in the samples was measured by means of a NH_3 pulse chemisorption method. To minimize the physisorption of NH_3, chemisorption was performed at 100 °C. As shown in Table 1, the number of acid sites in NbPSi-0.5 is comparable to those in NbP, HZSM-5, and NbPSi-1, even though large numbers of Nb atoms, which are associated with Lewis acidity, are substituted by Si atoms.

Figure 5 reveals NH_3 temperature programmed desorption (TPD) profiles for the catalysts. To determine the distribution of acid strength, the NH_3-TPD curves were deconvoluted by the Gaussian method, in which three peaks were used to indicate weak, medium, and strong acidity, respectively. The deconvolution results are listed in Table 2.

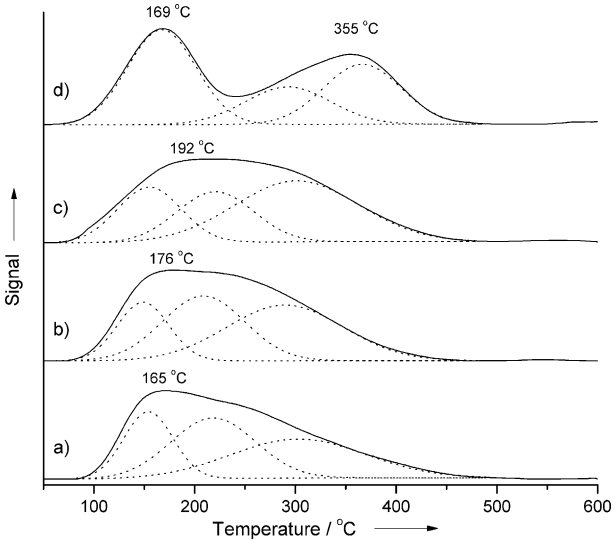

Figure 5. TPD profiles of adsorbed NH_3 on a) NbPSi-0.5, b) NbPSi-1, c) NbP, and d) HZSM-5.

Table 2. Deconvolution results of NH_3-TPD profiles for the catalysts.

Solid acid	A_{total}[a] [a.u.]	Weak acidity T_m[b] [°C]	Weak acidity X[c] [%]	Medium acidity T_m[b] [°C]	Medium acidity X[c] [%]	Strong acidity T_m[b] [°C]	Strong acidity X[c] [%]
NbPSi-0.5	62.5	154	24.1	218	37.5	302	38.4
NbPSi-1	65.8	155	23.4	216	34.1	300	42.5
NbP	69.6	155	23.3	220	25.5	301	51.2
HZSM-5	67.2	167	45.2	292	22.4	366	32.4

[a] Sum of the area of deconvoluted peaks. [b] Peak maximum temperature. [c] Peak fraction.

The peak maximum of NbPSi-0.5 appeared at a lower temperature than that of the other catalysts, indicating that the acidity of NbPSi-0.5 is weaker than that of other catalysts. In addition, among the NbP-based catalysts, NbPSi-0.5 showed a minimum density for strong acidity. These results are consistent with the in situ FTIR results, implying that the acidic center of NbPSi-0.5 is related to weak–medium acid sites.

Moreover, no significant differences between the total peak areas of the samples were found. This result is again in agreement with the NH_3 pulse chemisorption results, indicating that the number of acid sites on NbPSi-0.5 is similar to those for NbP and HZSM-5.

Table 3. Product selectivity for NbPSi-0.5, NbPSi-1, NbP, and HZSM-5.[a]

Product	Selectivity [%] NbPSi-0.5	NbPSi-1	NbP	HZSM-5
acrolein	76.3	70.5	65.6	76.6
hydroxyacetone (acetol)	15.8	7.3	6.8	5
acetaldehyde	0.4	3.2	5	4.7
acetone	0.8	3.8	4.7	4.2
propionaldehyde	1.7	3.4	5.2	0.4
propionic acid	0.2	1.5	1.1	2.4
others[b]	4.8	10.3	11.6	6.7

[a] Data are the mean values in the initial reaction period for 4 h. Reaction conditions: 250 °C and GHSV = 14940 mL $g_{catalyst}^{-1}$ h^{-1}. [b] Others include unidentified products and missing carbon.

Catalytic performance

The catalytic performance of NbPSi-0.5 for the dehydration of glycerol was investigated at 250 °C. First, the catalytic behavior of NbPSi-0.5 was compared with the corresponding values for NbP, NbPSi-1, and HZSM-5, and the results are displayed in Figure 6a and b. All of the catalysts achieved nearly complete conversion of glycerol at the initial stage of the reaction. The selectivity for acrolein (ca. 76%) over NbPSi-0.5 was similar to that for HZSM-5, whereas the acrolein selectivity over NbP and NbPSi-1 was about 12 and 6% lower, respectively, than those of others.

From Figure 6a, it can be clearly seen that the conversion over HZSM-5 and NbP steeply decreased to 31 and 51% after 8 h. Although NbPSi-1 showed longer stability than NbP and HZSM-5, the glycerol conversion over NbPSi-1 also decreased after 5 h. However, NbPSi-0.5 catalyzed the complete conversion of glycerol with a high selectivity for acrolein during the reaction, indicating the much higher stability and activity of NbPSi-0.5.

Furthermore, NbPSi-0.5 also showed quite a difference in the byproduct distribution compared to other catalysts. Data on product distribution can be found in Table 3. For NbPSi-0.5, hydroxyacetone was the main

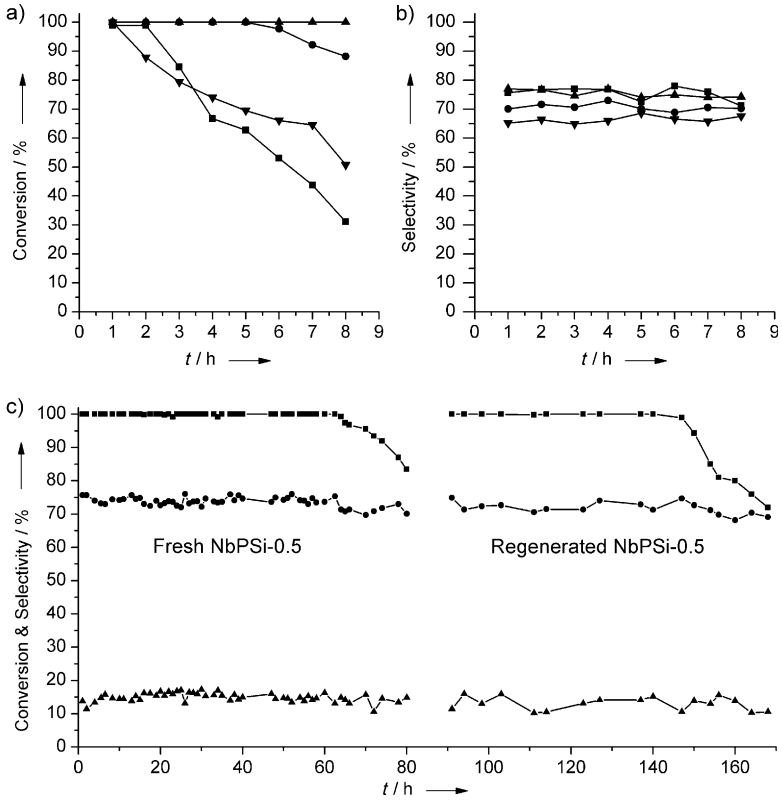

Figure 6. Time course for a) glycerol conversion and b) selectivity for acrolein over NbPSi-0.5 (▲), NbPSi-1 (●), NbP (▼), and HZSM-5 (■) at GHSV = 14940 mL $g_{catalyst}^{-1}$ h^{-1}. c) Stability results for glycerol conversion (■) and selectivity for acrolein (●) and hydroxyacetone (▲) over fresh and regenerated NbPSi-0.5 at GHSV = 12390 mL $g_{catalyst}^{-1}$ h^{-1}.

byproduct, and the selectivity for other byproducts did not exceed 1% (except for propionaldehyde). On the other hand, HZSM-5, NbP, and NbPSi-1 exhibited a lower selectivity for hydroxyacetone. Instead, they favored the formation of other byproducts, especially C_2 compounds, such as acetaldehyde. Acrolein and hydroxyacetone are both produced during the dehydration of glycerol, while the formation of other byproducts requires secondary reactions.[6] Therefore, the product distribution over NbPSi-0.5 suggests that, over NbPSi-0.5, the probabilities of the occurrence of secondary reactions are low.

To compare the stability of NbPSi-0.5 with that of the previously reported long-life catalyst more precisely, a long-term stability test was performed under the same conditions as those described in the literature.[16] As shown in Figure 6c, during a 70 h reaction, the complete conversion of glycerol over NbPSi-0.5 remained almost unchanged, and the selectivity for acrolein remained over 74%. This stability is about three times higher than that of the catalyst in the reference, which indicates a glycerol conversion of 78% after 24–25 h.[16] Moreover, it should be noted that NbPSi-0.5 produces a higher yield of acrolein (74%) after 24 h, although the acrolein selectivity of NbPSi-0.5 is slightly lower.

Although NbPSi-0.5 has a high stability and activity for this reaction, the regeneration and reuse of NbPSi-0.5 are preferred options for practical applications. Therefore, the possibility of regenerating the used NbPSi-0.5 was investigated by heat treatment under air conditions, a process that is intended to oxidize the coke formed on the catalysts. After the long-term stability test, the used NbPSi-0.5 was heated to 450 °C under an air flow (30 mL min^{-1}) for 4 h.

In the N_2 adsorption–desorption test (see Figure S2 in the Supporting Information), regenerated NbPSi-0.5 revealed an H1-type hysteresis loop, similar to fresh NbPSi-0.5. However, the hysteresis loop for regenerated NbPSi-0.5 was broader, and the pore size and BET surface area were slightly decreased after regeneration. A decrease in pore size was also observed in the TEM image (Figure S3 in the Supporting Information). These may be due to the partial collapse of pores during the regeneration process.

NH_3-TPD analyses were also performed to examine the acid properties of the regenerated NbPSi-0.5 (Figure S4 in the Supporting Information). The peak shape and maximum temperature of regenerated NbPSi-0.5 were consistent with those of fresh NbPSi-0.5, except for a small decrease in peak area. This indicates that the regeneration process does not change the acid strength and its distribution of NbPSi-0.5, but induces a slight decrease in the amount of acid sites.

In the catalytic test, regenerated NbPSi-0.5 also showed a high performance. Compared to fresh NbPSi-0.5, the regenerated NbPSi-0.5 exhibited almost the same selectivity for acrolein and the same glycerol conversion for about 40 h, although slightly faster deactivation was observed after 45 h. Katryniok et al. have recently reported similar results, indicating that regenerated catalysts had lower stability than fresh catalysts.[45] This can be attributed to heavy carbonaceous species, which are not oxidized under regeneration conditions.

Rationales for catalytic performance

The significantly enhanced catalytic performance of NbPSi-0.5 can be attributed to its favorable acidic and textural properties. The reaction network proposed by Corma et al. explains the formation of coke and its precursors by consecutive decomposition reactions starting from glycerol, acrolein, and hydroxyacetone.[9] Based on this mechanism and other literature data, it appears that dehydrogenation and hydrogenation comprise a large portion of those decomposition reactions and result in the production of various byproducts and coke precursors.[9,46] On the other hand, it has been reported that Brønsted acid sites are very inefficient in catalyzing the dehydrogenation of alcohols.[47] As shown above, NbPSi-0.5 possesses almost pure Brønsted acidity. This explains why NbPSi-0.5 facilitates the formation of dehydration products, but suppresses side reactions that can lead to the production of coke precursors. The product distribution over NbPSi-0.5 (Table 2) confirms this speculation. Over NbPSi-0.5, the total selectivity for acrolein and hydroxyacetone was more than 92%, and the concentrations of minor byproducts were very small.

Large mesopores of NbPSi-0.5 also play a role in enhancing the stability. As can be seen from the results given in Table 1, for HZSM-5 and NbP, the total pore volume and BET surface area decreased by more than 82 and 92%, and microporosity almost disappeared after the reaction. However, in the case of NbPSi-0.5, the total pore volume and BET surface area decreased by only 68 and 76%. NbPSi-1 also showed less decrease in the total pore volume and BET surface area than those of HZSM-5 and NbP. This difference is related to the fact that NbPSi-0.5 and NbPSi-1 have larger mesopores than those of HZSM-5 and NbP. The large mesoporosity may confer an advantage to NbPSi-0.5 in reducing pore blocking by carbon deposition, and as a result, the acid sites located inside the pores will still be available for long reactions. Similar beneficial effects of mesopores in deactivation can be found in the literature.[13,31]

In addition, NbPSi-0.5 showed different behaviors in terms of the properties of the carbonaceous deposits. The results of thermogravimetric (TG) and differential thermal analysis (DTA) for used NbPSi-0.5, NbPSi-1, NbP, and HZSM-5 are shown in Figure 7. Since the activities of the catalysts studied differ significantly with time, the amount of coke produced during an 8 h reaction is expressed as mg of coke per mmol of glycerol reacted. NbPSi-0.5 produced the smallest amount of coke among the used catalysts. It is well known that the strong acidity of catalyst is responsible for the formation of coke,[15,16,18] and the acidity of NbPSi-0.5 is slightly weaker than that of the others. Therefore, the weaker acid sites of NbPSi-0.5 can account for the lower coking tendency of NbPSi-0.5.

The DTA curves revealed two exothermic peaks in the temperature range of 250–600 °C, indicating the presence of two different types of coke in the used catalysts. The first peak, with a maximum at around 340–430 °C, can be assigned to easily oxidizable coke, whereas the second peak, with a maximum at above 500 °C, is related to the formation of more stable coke.[10,48] Compared with NbP, NbPSi-1, and HZSM-5, in

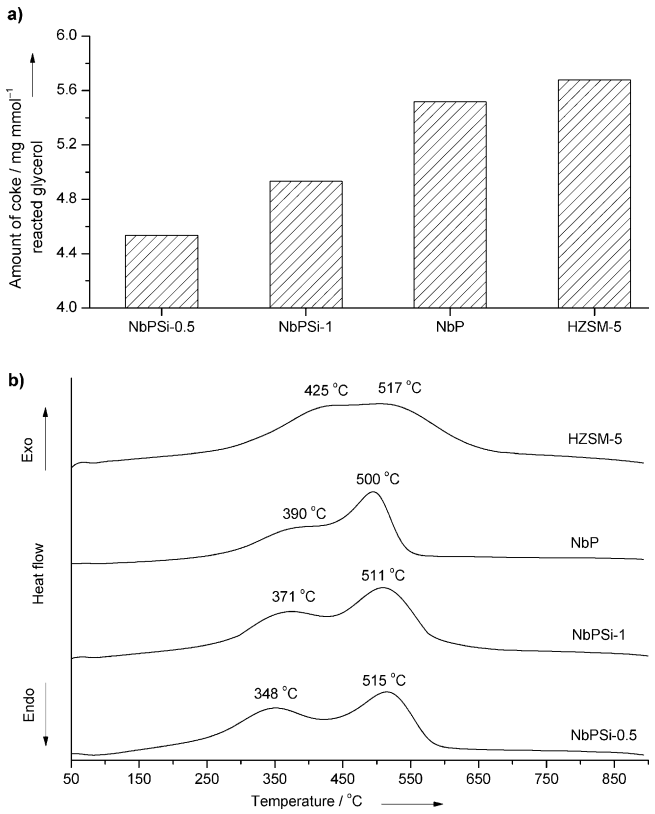

Figure 7. a) Amount of coke and b) DTA curves for used NbPSi-0.5, NbPSi-1, NbP, and HZSM-5.

the DTA curve for NbPSi-0.5, the maximum for the first peak occurred at a much lower temperature and the relative area ratio of the first to second peaks increased in the order of NbPSi-0.5 > NbPSi-1 > NbP > HZSM-5. These findings indicate that the coke produced over NbPSi-0.5 is made up of the more oxidizable form than those over other catalysts.

Analysis of the atomic H/C ratio in coke over the catalysts gives results consistent with the DTA data. The atomic H/C ratio in coke, as measured by CHNS elemental analysis, was found to be in the following order: NbPSi-0.5 (1.21) > NbPSi-1 (1.17) > NbP (1.08) > HZSM-5 (0.99). The higher H/C ratio of coked NbPSi-0.5 implies that the carbon deposits over NbPSi-0.5 have a less condensed and aromatized structure,[49] and therefore, are more readily oxidized.

Conclusions

This study reported a method for preparing a mesoporous siliconiobium phosphate (NbPSi-0.5) composite with a high content of Brønsted acidity and a demonstration of its potential for the efficient and stable dehydration of glycerol into acrolein. Importantly, NbPSi-0.5 was comprised of nearly pure Brønsted acid sites. In addition, NbPSi-0.5 contained comparable amounts of acid sites and exhibited weaker acidity than that of highly acidic NbP and the commercial zeolite HZSM-5. The findings also confirmed that NbPSi-0.5 had a well-developed mesoporous structure with large pores and a high surface area. Catalytic results showed that NbPSi-0.5 had a higher activity and stability than those of NbP and HZSM-5. Moreover, in long-term tests, the stability of NbPSi-0.5 was about three times as high as that of the reported long-life catalyst. The significantly enhanced catalytic performance of NbPSi-0.5 could be attributed to the following reasons: 1) the nearly pure Brønsted acidity promoted the production of main dehydration products, but suppressed side reactions leading to coke formation; 2) large mesopores significantly reduced pore blocking by coke deposition; and 3) the amount and oxidation temperature of produced coke decreased. These findings indicated that NbPSi-0.5 was a promising catalyst that could accelerate the practical viability of this reaction. We believe that NbPSi-0.5 can also be applicable to other acid-catalyzed reactions involving xylose, glucose, and so forth, as they are structurally analogous to glycerol.

Experimental Section

Preparation of catalysts: The mesoporous NbPSi-0.5 composite was synthesized by a solvothermal method combined with solvent evaporation. Solvothermal techniques are widely used for the synthesis of multicomponent materials,[50] and the solvent evaporation methods can be very useful for preparing mesostructured inorganic minerals.[51] Hence, to synthesize a mesostructured homogeneous composite of NbP and silicate, a combination of solvothermal treatment and solvent evaporation was developed. In addition, a small amount of diethylphosphatoethyltriethoxysilane, which contains both phosphate and silicate groups, was used to aid in producing a homogenous combination of components. $NbCl_5$, triethyl phosphate (TEP), ethanol, H_3PO_4 (85%) and tetraethyl orthosilicate (TEOS) were purchased from Sigma–Aldrich; diethylphosphatoethyltriethoxysilane (DEPETES, 95%) was from Gelest; and Pluronic P123 was from BASF. All chemicals were used as received.

In a typical synthesis, $NbCl_5$ (0.015 mol), TEP (0.0135 mol), and DEPETES (0.0015 mol) were dissolved in EtOH (85 mol). The dissolution of $NbCl_5$ in EtOH was performed in a glove box to avoid moisture contamination. A stirred solution of P123 (0.0006 mol) and H_3PO_4 (0.015 mol) in EtOH (115 mol) was then added. After stirring the mixture at 40 °C for 3 h, TEOS (0.015 mol) was added and the solution was stirred at 40 °C for 24 h. The resulting solution was then loaded into an autoclave and heated with continuous stirring at 150 °C for 24 h. The as-prepared pale white sol was transferred into a dish. The ethanol solvent was evaporated without controlling the humidity at 80 °C for 24 h. The resulting solids were calcined at 550 °C for 4 h.

For comparison with NbPSi-0.5, NbPSi-1 (atomic ratio Nb/P = 1) was prepared by processes identical to those of NbBSi-0.5, except for the content of $NbCl_5$. To obtain the atomic ratio of Nb/P = 1, 0.03 mol of $NbCl_5$ was used.

Pure NbP was also prepared according to a previously reported method.[33] HZSM-5 was prepared through the calcination of commercial zeolite NH_4ZSM-5 (zeolyst, $SiO_2/Al_2O_3 = 50$) at 500 °C for 6 h.

Characterization: The N_2 adsorption–desorption isotherms were recorded on a Micrometrics ASAP-2010 system. The pore size was calculated from the adsorption branches of isotherms by using BJH methods. The TEM and energy-dispersive X-ray spectroscopy (EDS) observations were carried out by using a JEOL JEM-3010 microscope operating at 300 kV. The elemental analysis of the bulk phase was performed by ICP-AES (Shimadzu, JP/ICPS-7500). The

XPS spectra were measured with a Kratos AXIS-His electron spectrometer equipped with a MgK_α X-ray source and a hemispherical electron energy analyzer. The structural FTIR spectra of samples were obtained by using a Nicolet 6700 FT-IR spectrophotometer. In situ FTIR spectra of NH_3 adsorption were measured with a Midac spectrometer (model 2100). A self-supported pellet containing about 40 mg of the sample was placed in an in situ IR cell, designed by Moon et al.[52] The pellet was pretreated at 150 °C under N_2 flow for 1 h. After cooling to room temperature, the pellet was exposed to NH_3 gas at 2.67 kPa for 3 min. The desorption of NH_3 was performed by evacuation at different temperatures (30, 100, 200, and 280 °C). The spectrum was recorded after desorption at each temperature. The NH_3-pulse chemisorption was carried out by using a Micrometrics Autochem II chemisorption analyzer. Prior to analysis, 0.1 g of sample was pretreated under He flow at 500 °C for 1 h. After cooling to 100 °C, 10.2% NH_3/He gas was periodically injected onto the sample by using an injection loop. The amount of NH_3 uptake was monitored by a thermal conductivity detector (TCD) until successive peaks showed the same area. The NH_3-TPD spectra were obtained by using the same analyzer and pretreatment procedure as that used for NH_3-pulse chemisorption. The samples were saturated with 10.2% NH_3/He gas at 50 °C. Physisorbed NH_3 was eliminated by flushing with a stream of He at 100 °C. After again cooling to 50 °C, the temperature was increased to 800 °C at a rate of 10 °C min^{-1} under a stream of He. TG and DTA were performed simultaneously in a TA instruments SDT Q600 analyzer. The experiments were carried out from room temperature to 800 °C with a heating rate of 10 °C min^{-1} under air. The atomic H/C ratio of coke over the used catalysts was determined by CHNS elemental analysis by using a LECO CHNS-932 instrument.

Catalytic reaction: The dehydration of glycerol was performed under atmospheric pressure at 250 °C. A catalyst sample of 0.3 g was packed into a quartz reactor (8 mm inner diameter), and the reactor was then placed in an electric furnace. The temperature of the catalyst bed was monitored by a K-type thermocouple and controlled by a PID controller. Before the reaction, the catalyst was preheated to the reaction temperature under a N_2 flow (30 mL min^{-1}) for 1 h. A 10 wt% aqueous solution of glycerol was injected into the vaporizer by using a syringe pump. The reactant vapor was diluted with a stream of N_2 (30 mL min^{-1}) in the vaporizer and then fed into the catalyst bed. The aqueous solution of glycerol was injected at a rate of 2.1 mL h^{-1} to obtain a molar composition of glycerol/H_2O/N_2 = 1.3/53.6/40.2 and a GHSV of 14940 mL $g_{catalyst}^{-1}$ h^{-1}. In the case of the long-term reaction, the solution of glycerol was fed at a rate of 1.5 mL h^{-1}, giving a molar composition of glycerol/H_2O/N_2 = 1.1:50.5:48.4 and a GHSV of 12390 mL $g_{catalyst}^{-1}$ h^{-1}. The reaction product was collected in a cold trap and analyzed by a gas chromatograph (Younglin ACME 6100 model) equipped with a FID detector and a HP-Innowax capillary column. To ensure the identification of products, GC-MS analyses were also carried out by using an Agilent 7890A GC system equipped with an Agilent 5975C MS detector and a HP-5ms capillary column.

Acknowledgements

This work was financially supported by a grant from the Industrial Source Technology Development Programs (10033352) of the Ministry of Knowledge Economy (MKE) of Korea. This research was also supported by the World Class University program funded by the Ministry of Education, Science, and Technology through the National Research Foundation of Korea (R31-10013).

Keywords: Brønsted acids · dehydration · heterogeneous catalysis · mesoporous materials · renewable resources

[1] R. Rinaldi, F. Schüth, *Energy Environ. Sci.* **2009**, *2*, 610 – 626.
[2] M. Hara, *Energy Environ. Sci.* **2010**, *3*, 601 – 607.
[3] J. N. Chheda, G. W. Huber, J. A. Dumesic, *Angew. Chem.* **2007**, *119*, 7298 – 7318; *Angew. Chem. Int. Ed.* **2007**, *46*, 7164 – 7183.
[4] E. Taarning, C. M. Osmundsen, X. Yang, B. Voss, S. I. Andersen, C. H. Christensen, *Energy Environ. Sci.* **2011**, *4*, 793 – 804.
[5] R. Weingarten, G. A. Tompsett, W. C. Conner, Jr., G. W. Huber, *J. Catal.* **2011**, *279*, 174 – 182.
[6] B. Katryniok, S. Paul, V. Belliere-Baca, P. Rey, F. Dumeignil, *Green Chem.* **2010**, *12*, 2079 – 2098.
[7] B. Katryniok, S. Paul, M. Capron, F. Dumeignil, *ChemSusChem* **2009**, *2*, 719 – 730.
[8] S. H. Chai, H. P. Wang, Y. Liang, B. Q. Xu, *Green Chem.* **2007**, *9*, 1130 – 1136.
[9] A. Corma, G. W. Huber, L. Sauvanaud, P. O'Connor, *J. Catal.* **2008**, *257*, 163 – 171.
[10] C. J. Jia, Y. Liu, W. Schmidt, A. H. Lu, F. Schüth, *J. Catal.* **2010**, *269*, 71 – 79.
[11] Y. T. Kim, K. D. Jung, E. D. Park, *Microporous Mesoporous Mater.* **2010**, *131*, 28 – 36.
[12] K. Pathak, K. M. Reddy, N. N. Bakhshi, A. K. Dalai, *Appl. Catal. A* **2010**, *372*, 224 – 238.
[13] C. J. Zhou, C. J. Huang, W. G. Zhang, H. S. Zhai, H. L. Wu, Z. S. Chao, *Stud. Surf. Sci. Catal.* **2007**, *165*, 527 – 530.
[14] A. Alhanash, E. F. Kozhevnikova, I. V. Kozhevnikov, *Appl. Catal. A* **2010**, *378*, 11 – 18.
[15] S. H. Chai, H. P. Wang, Y. Liang, B. Q. Xu, *Green Chem.* **2008**, *10*, 1087 – 1093.
[16] B. Katryniok, S. Paul, M. Capron, C. Lancelot, V. Bellière-Baca, P. Rey, F. Dumeignil, *Green Chem.* **2010**, *12*, 1922 – 1925.
[17] E. Kraleva, R. Palcheva, L. Dimitrov, U. Armbruster, A. Brückner, A. Spojakina, *J. Mater. Sci.* **2011**, *46*, 7160 – 7168.
[18] E. Tsukuda, S. Sato, R. Takahashi, T. Sodesawa, *Catal. Commun.* **2007**, *8*, 1349 – 1353.
[19] P. Lauriol-Garbay, J. M. M. Millet, S. Loridant, V. Bellière-Baca, P. Rey, *J. Catal.* **2011**, *280*, 68 – 76.
[20] L. Z. Tao, S. H. Chai, Y. Zuo, W. T. Zheng, Y. Liang, B. Q. Xu, *Catal. Today* **2010**, *158*, 310 – 316.
[21] A. Ulgen, W. Hoelderich, *Catal. Lett.* **2009**, *131*, 122 – 128.
[22] Q. Liu, Z. Zhang, Y. Du, J. Li, X. Yang, *Catal. Lett.* **2009**, *127*, 419 – 428.
[23] F. Wang, J. L. Dubois, W. Ueda, *J. Catal.* **2009**, *268*, 260 – 267.
[24] F. Wang, J. Xu, J. L. Dubois, W. Ueda, *ChemSusChem* **2010**, *3*, 1383 – 1389.
[25] I. Nowak, M. Ziolek, *Chem. Rev.* **1999**, *99*, 3603 – 3624.
[26] M. Ziolek, *Catal. Today* **2003**, *78*, 47 – 64.
[27] S. Okazaki, N. Wada, *Catal. Today* **1993**, *16*, 349 – 359.
[28] P. Carniti, A. Gervasini, S. Biella, A. Auroux, *Catal. Today* **2006**, *118*, 373 – 378.
[29] T. Armaroli, G. Busca, C. Carlini, M. Giuttari, A. M. R. Galletti, G. Sbrana, *J. Mol. Catal. A* **2000**, *151*, 233 – 243.
[30] K. Nakajima, Y. Baba, R. Noma, M. Kitano, J. N. Kondo, S. Hayashi, M. Hara, *J. Am. Chem. Soc.* **2011**, *133*, 4224 – 4227.
[31] L. G. A. van de Water, J. C. van der Waal, J. C. Jansen, T. Maschmeyer, *J. Catal.* **2004**, *223*, 170 – 178.
[32] H. Zhu, Z. Liu, D. Kong, Y. Wang, Z. Xie, *J. Phys. Chem. C* **2008**, *112*, 17257 – 17264.
[33] N. K. Mal, M. Fujiwara, *Chem. Commun.* **2002**, 2702 – 2703.
[34] J. Zhu, Y. Huang, *Inorg. Chem.* **2009**, *48*, 10186 – 10192.
[35] S. V. Karpov, E. V. Kolobkova, *Fiz. Khim. Stekla* **1991**, *17*, 425 – 434.
[36] R. M. Pittman, A. T. Bell, *J. Phys. Chem.* **1993**, *97*, 12178 – 12185.
[37] G. Connell, J. A. Dumesic, *J. Catal.* **1987**, *105*, 285 – 298.

[38] M. H. C. de La Cruz, A. S. Rocha, E. R. Lachter, A. M. S. Forrester, M. C. Reis, R. A. S. S. Gil, S. Caldarelli, A. D. Farias, W. A. Gonzalez, *Appl. Catal. A* **2010**, *386*, 60 – 64.
[39] C. Dayanand, G. Bhikshamaiah, V. J. Tyagaraju, M. Salagram, A. S. R. K. Murthy, *J. Mater. Sci.* **1996**, *31*, 1945 – 1967.
[40] H. El Rassy, A. C. Pierre, *J. Non-Cryst. Solids* **2005**, *351*, 1603 – 1610.
[41] G. V. A. Martins, G. Berlier, C. Bisio, S. Coluccia, H. O. Pastore, L. Marchese, *J. Phys. Chem. C* **2008**, *112*, 7193 – 7200.
[42] C. C. Hwang, C. Y. Mou, *J. Phys. Chem. C* **2009**, *113*, 5212 – 5221.
[43] Q. Sun, A. Auroux, J. Shen, *J. Catal.* **2006**, *244*, 1 – 9.
[44] F. Lónyi, J. Valyon, *Microporous Mesoporous Mater.* **2001**, *47*, 293 – 301.
[45] B. Katryniok, S. Paul, M. Capron, V. Bellière-Baca, P. Rey, F. Dumeignil, *ChemSusChem* **2012**, *5*, 1298 – 1306.
[46] P. Lauriol-Garbey, G. Postole, S. Loridant, A. Auroux, V. Belliere-Baca, P. Rey, J. M. M. Millet, *Appl. Catal. B* **2011**, *106*, 94 – 102.
[47] C. P. Bezouhanova, M. A. Al-Zihari, *Catal. Lett.* **1991**, *11*, 245 – 248.
[48] H. Atia, U. Armbruster, A. Martin, *J. Catal.* **2008**, *258*, 71 – 82.
[49] M. Guisnet in *Handbook of Heterogeneous Catalysis, Vol. 2* (Eds.: G. Ertl, H. Knözinger, J. Weitkamp), Wiley-VCH, Weinheim, **1997**, pp. 626 – 632.
[50] S. Feng, L. Guanghua in *Modern Inorganic Synthetic Chemistry* (Eds.: R. Xu, W. Pang, Q. Huo), Elsevier, Amsterdam, **2011**, pp. 63 – 95.
[51] S. W. Boettcher, J. Fan, C. K. Tsung, Q. Shi, G. D. Stucky, *Acc. Chem. Res.* **2007**, *40*, 784 – 792.
[52] S. H. Moon, H. Windawi, J. R. Katzer, *Ind. Eng. Chem. Fundam.* **1981**, *20*, 396 – 399.

Received: August 10, 2012
Published online on November 6, 2012

